Available online at www.sciencedirect.com

SciVerse ScienceDirect

Ceramics International 39 (2013) 3157–3163

CERAMICS INTERNATIONAL

www.elsevier.com/locate/ceramint

Effect of fibered morphology on the properties of Al_2O_3 nanoceramic films

Su-Shia Lin*

Department of Applied Materials and Optoelectronic Engineering, National Chi Nan University, No. 1 University Road, Puli, Nantou Hsien 54561, Taiwan, ROC

Received 11 August 2012; received in revised form 28 September 2012; accepted 28 September 2012
Available online 5 October 2012

Abstract

The Al_2O_3 nanoceramic films were deposited by rf magnetron sputtering. The formation of fibered morphology of Al_2O_3 film was dominated by decreasing Ar pressure, and was good for the hydrophilicity of the deposited film. The nonlinear refractive indices of Al_2O_3 films deposited on the glass substrates were measured by Moiré deflectometry, and were of the order of 10^{-8} cm^2 W^{-1}. For the Al_2O_3 film deposited in a mixed Ar–O_2 atmosphere, the diffusion of oxygen into the grains could smooth the thin film and enhanced the transmission. The Al_2O_3 film exhibiting fibered morphology corresponded to higher optical energy gap and higher transmission in the VIS–NIR region. As the results, the surface morphologies affected the hydrophilicity and optical properties of Al_2O_3 films significantly.

Keywords: Optical properties; Sputtering; Morphology; Hydrophilicity

1. Introduction

Aluminum oxide thin films are widely used in many mechanical, optical and microelectronic applications because of their excellent properties in terms of chemical inertness, mechanical strength and hardness, transparency, high abrasion and corrosion resistance, and insulating and optical properties [1,2]. However, the properties of thin films are dependent on the processing parameters [3]. Different applications and environments demand different kinds of properties of the thin films. For optical devices, aluminum oxide is a very promising layer material because of its interesting optical properties and low cost [4]. However, there is a relationship between surface morphology and optical property, which needs to be further investigated.

Aluminum oxide thin films have been prepared by several techniques, including sol–gel method [5], spray pyrolysis [6], chemical vapor deposition [7], atomic layer deposition [8] and sputtering [9]. In this study, Al_2O_3 nanoceramic films were deposited by rf magnetron sputtering without heating the substrates. The influence of working pressure on the fibered morphologies of Al_2O_3 films with respect to the hydrophilicity and optical properties was investigated.

Transparent materials generally exhibit the optical Kerr effect. Nonlinear refractive indices of materials are of great interest because of potential applications in designing optical devices and laser technology [10–13]. Moiré deflectometry is a powerful tool for measuring the nonlinear refractive indices of materials. The main advantages of the Moiré deflectometry technique are its extreme experimental simplicity, lower cost and lower sensitivity to external disturbances than other interferometric methods. In this study, this method was applied to measure the nonlinear refractive indices of Al_2O_3 films on glass substrates under illumination with a 5-mW He–Ne laser ($\lambda = 632.8$ nm).

2. Experimental procedures

The Al_2O_3 nanoceramic films were deposited on glass (Corning 1737) by rf magnetron sputtering. The target used in this study was sintered stoichiometric Al_2O_3 (99.99% purity, 5 cm diameter, 5 mm thickness, Target

*Tel.: +886 49 2910960x4771; fax: +886 49 2912238.
E-mail address: sushia@ncnu.edu.tw

0272-8842/$ - see front matter © 2012 Elsevier Ltd and Techna Group S.r.l. All rights reserved.
http://dx.doi.org/10.1016/j.ceramint.2012.09.099

Materials Inc., USA). The dimension of the glass substrates was 24 mm × 24 mm × 1.1 mm. Before deposition, the substrates were ultrasonically cleaned in alcohol, rinsed in deionized water and dried in nitrogen. A turbo-molecular pump backed by a rotary pump, was used to achieve a base pressure of 1.3×10^{-4} Pa. The sputtering was performed in a pure Ar or a mixed Ar–O_2 atmosphere with a target-to-substrate distance of 15 cm. The chamber was back-filled with a pure Ar atmosphere at a working pressure of 0.087–0.36 Pa, or a mixed Ar–O_2 atmosphere at a working pressure of 0.36 Pa. For the deposition of the films, the substrates were not heated. An rf power (13.56 MHz, RGN-1302, ULVAC, Japan) of 200 W was supplied to the Al_2O_3 target. No external bias voltage was applied to the substrate. The rotating speed of the substrate was 20 rpm, and the thickness of films was maintained at 100 nm.

The film thickness was measured using a surface profiler (Alpha-Step 500, TENCOR, Santa Clara, CA). X-ray diffraction (XRD; Rigaku D/MAX2500, Japan) was used to study the crystal structure. The surface morphologies and surface roughness were examined by atomic force microscopy (AFM; Agilent 5500, Santa Clara, CA). The water contact angles on samples were measured by contact angle meter (Model 100SB, Sindatek, Taiwan). The optical transmission spectra of films in the visible–near infrared (VIS–NIR) region were obtained using a spectrophotometer (HP 8452 A diode array spectrophotometer, Hewlett Packard, Palo Alto, CA). Linear refractive indices of samples were recorded using a spectrometer (MP100-ST, Fremont, CA). Stress was measured by the Nano Indenter XP System (MTS Systems Corporation, MN, USA).

Fig. 1 shows the Moiré deflectometry experimental setup that is used to measure the nonlinear refractive indices of Al_2O_3 films on glass substrates. Lens L_1 focused a 5-mW He–Ne laser beam (wavelength of 632.8 nm), which was re-collimated by lens L_2. The focal lengths of lenses L_1, L_2 and L_3 were all -250 mm. Two similar Ranchi gratings, G_1 and G_2 with a pitch of 0.1 mm were used to construct the Moiré fringe patterns. The distance between the planes of G_1 and G_2 was set to 64 mm, which is one of the Talbot distances of the used gratings. The Talbot distances satisfy $z_t = tp^2/\lambda$ where p is the periodicity of the grating; λ is the wavelength of light, and t is an integer. In this work, the Moiré fringes were clearly formed at a Talbot distance of $z_{t=4} \approx 64$ mm. The Moiré fringe patterns were projected onto a computerized CCD camera by lens L_3, which was placed at the back of the second grating.

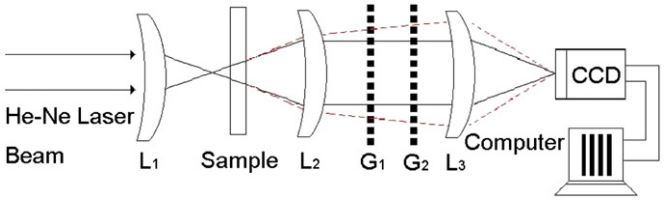

Fig. 1. The experimental setup for measuring nonlinear refractive index by the Moiré deflectometry technique.

3. Results and discussion

Fig. 2 shows the morphologies of Al_2O_3 films deposited at different pressures. In Fig. 2a and b, Al_2O_3 films were composed of irregular fibers with width of 50–150 nm, and included a few pores. The fibered morphology is a consequence of the nucleation of grains that grow geometrically and impinge laterally. It is a result of a competition during deposition between the rate of arrival of new Al_2O_3

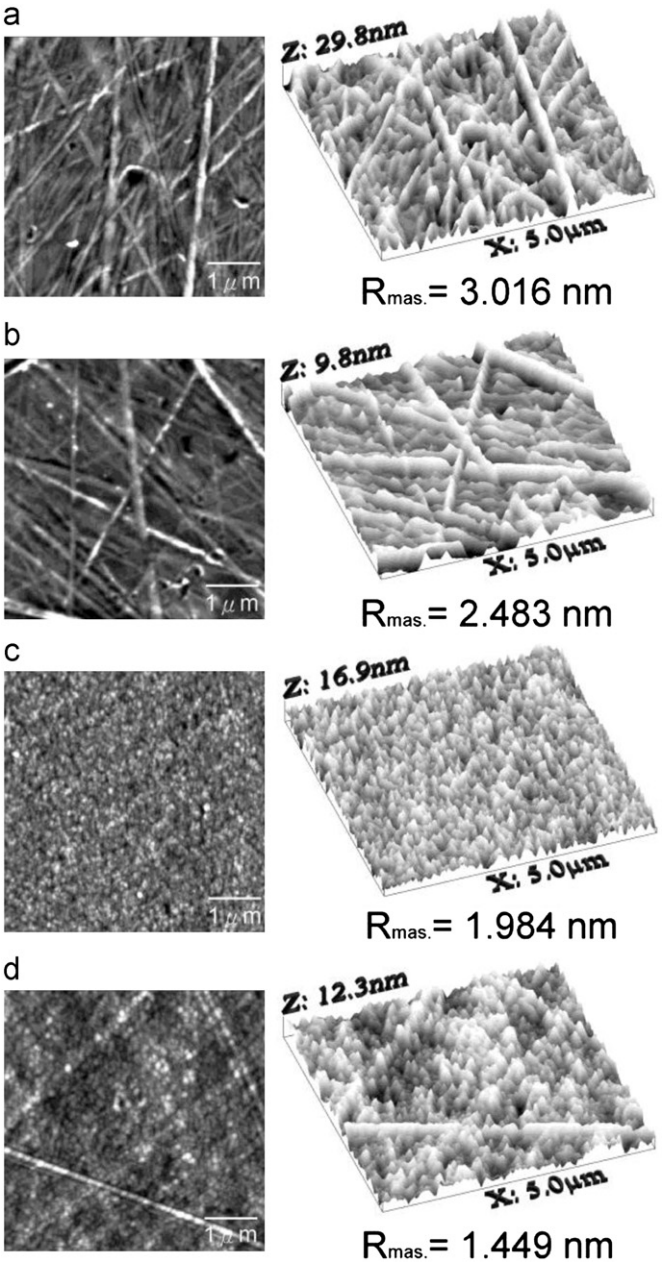

Fig. 2. The morphologies of Al_2O_3 films deposited at pressures of (a) 0.15 Pa (Ar); (b) 0.29 Pa (Ar); (c) 0.36 Pa (Ar) and (d) 0.36 Pa (Ar 0.29 Pa + O_2 0.07 Pa).

species on the surface and the concurrent redistribution over the surface by diffusion. Hence, the fibered morphology may be due to the nonequilibrium growth.

The total energy in a film deposited on a substrate is the sum of three components: (i) surface energy of the film, (ii) film–substrate interfacial energy, and (iii) strain energy in the film. The film generally grows with the plane parallel to the substrate surface, which minimizes the surface free energy of the film [14]. Films are often deposited on substrates, which results in different thermal properties for the films themselves. This could lead to strain in the films, particularly if they were deposited at elevated temperatures [14]. For the growth of all films, the total energy is minimized [14].

According to the kinetics of grain growth [15,16], the growing faces of a grain are parts of the free surface of the film. These grain faces corresponding to the final grain shape are determined by the orientation of the grain. A growth competition can start among the neighboring grains in case of different orientation according to the types of their growing faces. The faster growing grains will grow over the slower growing ones. This competition terminates when only grains exhibiting the same type of grain faces proceed to the free surface. This competitive grain growth represents an orientation selection among the grains, and results in the growth of fibered structure. This happens when atoms or molecules in the deposit are bonded more strongly to each other than to the substrate.

In the Al_2O_3 films, the nuclei are randomly oriented and the fibers are evolutionary fibers due to selection mechanisms. This selection can be related either to the competitive growth of grains or to the abnormal grain growth controlled by the minimum of the surface energy and interfacial energy [17]. The complete coalescence of the contacting grains is a periodic process during the film growth. Besides the increase of grain size, it results also in the changes of grain orientations owing to lowering the free energy of the developing grains. Therefore, the homogeneous grains with grain size of 50–100 nm were observed by increasing Ar pressure as shown in Fig. 2c.

According to Fig. 2a–c, the collisions of these particles with the growing film could smooth the thin film by surface diffusion mechanism, and enhanced surface atom mobility [3,18]. Because the probability of collisions of particles increased by increasing working pressure, it is probably why Al_2O_3 film deposited at higher pressure had more adatom mobility and the relatively low surface roughness. Therefore, the surface morphologies of Al_2O_3 films displayed homogeneous grains and no fibered structures at Ar pressure of 0.36 Pa.

By comparing Fig. 2c with d, a few fibered structures exhibited in Fig. 2d. The sputter yield is defined as the number of atoms or molecules ejected from a target surface per incident ion and is a measure of the efficiency of sputtering [19]. In this study, sputtering gas is Ar. Therefore, the equilibrium growth of Al_2O_3 film was mainly dominated by increasing Ar pressure to 0.36 Pa. The probability of collisions of particles increased by mixing oxygen atmosphere, which could smooth the thin film by surface diffusion mechanism and enhanced surface atom mobility [20]. It was probably why the surface roughness of Al_2O_3 film decreased by mixing oxygen atmosphere.

Fig. 3 shows the X-ray diffraction patterns of Al_2O_3 films deposited at various pressures. XRD analysis was conducted on the films using a Rigaku D/ MAX2500 goniometer with 18 kW rotating anode X-ray, equipped with a thin film attachment unit. The equipment was operated with CuK_α ($\lambda = 1.5418$ Å) radiation at 40 kV, 100 mA and a scanning speed of 4° min^{-1} at an incident angle of 3°. The interval of the scan was 0.01° and the scanning range was 10°–70°. In Fig. 3, it can be found that there is a broad diffraction peak (1 1 0) corresponding to nanocrystalline θ–Al_2O_3. The Al_2O_3 film with the fibered morphology showed stronger peak (1 1 0) owing to lower Ar pressure. It indicated that the nanocrystallinity was enhanced by fibered morphology.

Fig. 4 shows water contact angles on Al_2O_3 films deposited at various pressures. Wettability of a solid surface with liquids is not only governed by its chemical

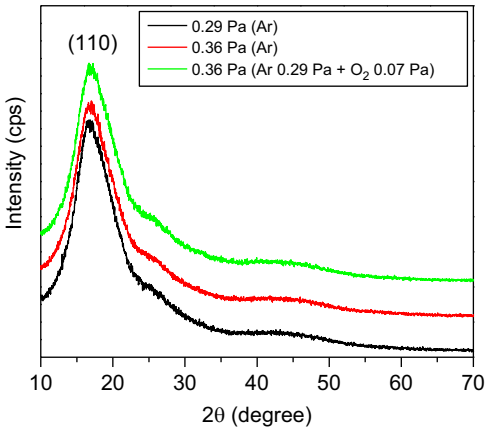

Fig. 3. The X-ray diffraction patterns of Al_2O_3 films deposited at various pressures.

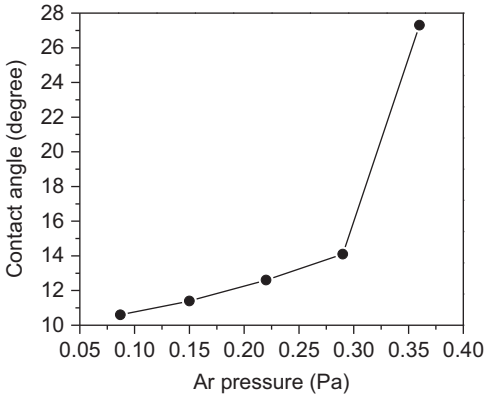

Fig. 4. Water contact angles on Al_2O_3 films deposited at various pressures.

properties but also by its geometry. Hydrophilicity is well known to be enhanced by fine roughness [21,22]. Therefore, a control of surface microstructure of the films is a way to enhance the hydrophilicity. The hydrophilicity of Al_2O_3 films was evaluated by examining the water contact angles on Al_2O_3 films. The water contact angle decreased by decreasing Ar pressure. It suggested that the hydrophilicity of Al_2O_3 film was enhanced by fibered morphology.

All optical properties are as a result of the interaction of electromagnetic radiation with the electrons of the material [23]. The optical energy gap E_g could be obtained from the intercept of $(\alpha h\nu)^2$ versus hν for direct allowed transitions [24]. Better linearity was observed for $(\alpha h\nu)^2$ versus $h\nu$ [24,25] as shown in Fig. 5. Fig. 5 shows plots of $(\alpha h\nu)^2$ versus $h\nu$ for Al_2O_3 films deposited at various pressures. The optical energy gap decreased with the increase of Ar pressure or O_2 pressure, especially Ar pressure, but not much. The change of optical energy gap by increasing Ar pressure or O_2 pressure has been interpreted as a Moss–Burstein shift, where the change is the result of the decrease in the free carrier concentration, and the corresponding downward shift of the Fermi level to below the band edge [26,27]. According to Figs. 2 and 5, it suggested that the Al_2O_3 film with fibered morphology showed higher optical energy gap.

Fig. 6 shows the transmission in the VIS–NIR region of Al_2O_3 films deposited at various pressures. The optical transmission in the VIS–NIR region all exceeded 95%. The transmission in the VIS–NIR region increased with the decrease of Ar pressure. When an interaction occurs between the photon and the electron, the electron crosses the energy gap E_g from the filled valence-band level to the unfilled conduction-band states. Because the optical energy gap of Al_2O_3 film deposited at lower Ar pressure was higher, the transmission of Al_2O_3 film was higher.

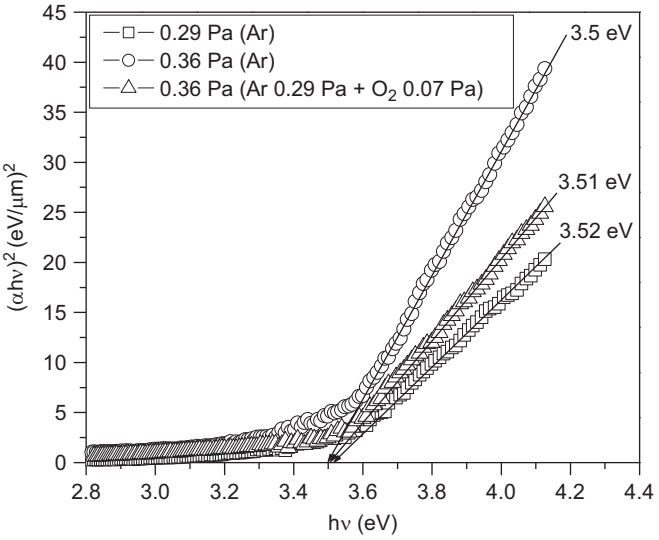

Fig. 5. Plots of $(\alpha h\nu)^2$ versus hν for Al_2O_3 films deposited at various pressures.

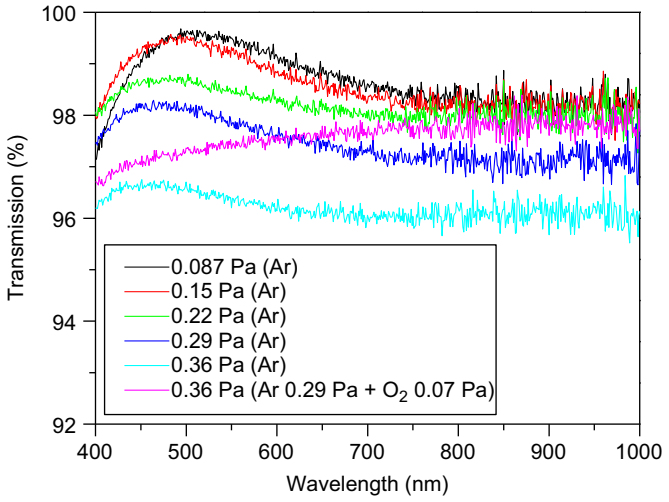

Fig. 6. The transmission in the VIS–NIR region of Al_2O_3 films deposited at various pressures.

According to Figs. 2 and 6, the Al_2O_3 films exhibiting fibered morphologies corresponded to higher transmission. This result suggested that the fibered morphology was good for the transmission in the VIS–NIR region of Al_2O_3 film. In addition, the excess oxygen could be trapped in the interfaces between grains, and the optical transmission could be improved [20,28]. Therefore, the diffusion of oxygen into the grains enhanced the transmission when the Al_2O_3 film deposited in a mixed Ar–O_2 atmosphere.

The refractive index, n, which depends on the radiation intensity, may be expressed in terms of the nonlinear refractive index n_2 ($cm^2\ W^{-1}$):

$$n(r,z) = n_o + n_2 I(r,z) = n_o + \Delta n(r,z) \quad (1)$$

where n_o is the linear refractive index, $I(r, z)$ is the irradiance of the laser beam within the sample, and $\Delta n(r, z)$ is the light-induced change in refractive index. Based on the assumption that a Gaussian beam is traveling in the $+z$ direction, the beam irradiance can be written as

$$I(r,z) = I_0 \frac{\omega_0^2}{\omega^2(z)}\left[1 - \frac{2r^2}{\omega^2(z)}\right] \quad (2)$$

where r is the radial radius of the imaginary sphere; ω_0 is the spot size of the beam at the focus; $\omega(z) = \omega_0(1 + z^2/z_0^2)^{1/2}$ is the beam radius at a distance z from the position of the waist; $z_0 = \pi\omega_0^2/\lambda$ is the diffraction length of the Gaussian beam, and λ is the wavelength. The irradiance of the beam at the focus is denoted I_0 and in terms of the input laser power, p_{in}, which equals $2p_{in}/\pi\omega_0^2$. Therefore, for a Gaussian laser beam, the radial dependence of the irradiance gives rise to a radially-dependent parabolic refractive index change near the beam axis:

$$\Delta n(r,z) = n_2 I_0 \frac{\omega_0^2}{\omega^2(z)}\left[1 - \frac{2r^2}{\omega^2(z)}\right] \quad (3)$$

Moiré deflectometry is a sensitive technique for measuring changes in the refractive indices of materials. The sensitivity of this technique is determined by the minimum

measurable-angle of rotation (α_{min}). The tested sample was placed at various distances from the focal point of lens L_1, and the minimum angle of rotation was obtained. The same experiment was performed by using only a pure glass substrate to check the contribution of the glass substrate to the nonlinear refraction measurement. No observed fringe rotation or change in fringe size was found.

For the thin nonlinear medium of thickness d, the lowest nonlinear refractive index can be written as

$$n_{2,\min} = \frac{\theta f_2^2}{2z_t}\frac{f_2^2\pi\omega_0^4}{2dp_{\text{in}}z_0^2}\alpha_{\min} \tag{4}$$

and the change in the minimum refractive index is

$$\Delta n_{\min} = \frac{\theta}{z_t}\frac{f_2^2\omega_0^2}{dz_0^2}\alpha_{\min} \tag{5}$$

Fig. 7 shows the minimum nonlinear refractive indices and the change in the minimum refractive indices of Al_2O_3 films deposited at various pressures on glass substrates. The nonlinear refractive index was measured to be of the order of 10^{-8} cm^2 W^{-1} and the change in refractive index was of the order of 10^{-5}.

Fig. 8 shows the Moiré fringe patterns of Al_2O_3 films deposited at pressures of (a) 0.29 Pa (Ar); (b) 0.36 Pa (Ar) and (c) 0.36 Pa (Ar 0.29 Pa+O_2 0.07 Pa). According to Fig. 8a–c, the Moiré fringes exhibited no rotation or change in size, suggesting that pressure did not significantly change the number of pores in Al_2O_3 films. In Fig. 8a and c, the Moiré fringe patterns were brighter than Fig. 8b. It was probably due to the fibered morphologies of Al_2O_3 films.

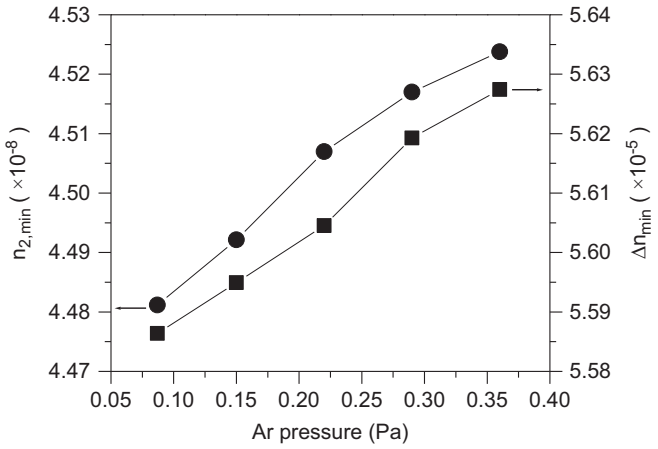

Fig. 7. The minimum nonlinear refractive indices and the change in the minimum refractive indices of Al_2O_3 films deposited at various pressures on glass substrates.

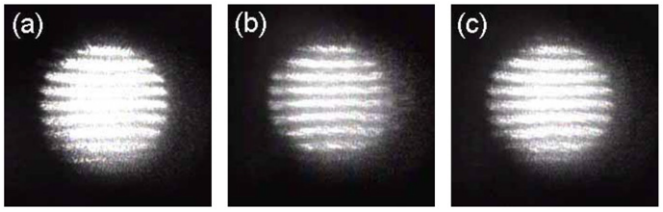

Fig. 8. The Moiré fringe patterns of Al_2O_3 films deposited at pressures of (a) 0.29 Pa (Ar); (b) 0.36 Pa (Ar) and (c) 0.36 Pa (Ar 0.29 Pa+O_2 0.07 Pa).

A change of the linear refractive index caused by stress is called the photoelastic effect [29]. The linear refractive index is specified by the indicatrix, which is an ellipsoid whose coefficients are the components of the relative dielectric impermeability tensor B_{ij} at optical frequencies:

$$B_{ij}x_ix_j = 1 \tag{6}$$

The small change of the linear refractive index produced by stress is a small change in the shape, size and orientation of the indicatrix. This change is specified by the small changes in the coefficients B_{ij}.

If terms of higher-order than the first in the field of stresses are neglected, then the changes ΔB_{ij} in the coefficients are

$$\Delta B_{ij} = \varphi_{ijkl}\sigma_{kl} \quad or\ \Delta B_{ij} = p_{ijrs}\varepsilon_{rs} \tag{7}$$

where φ_{ijkl} and p_{ijrs} are called the piezo-optical and strain-optical coefficients, which typically have the orders of magnitude of 10^{-12} Pa^{-1} and 10^{-1} Pa^{-1}, respectively.

Based on the relation, $B=1/n_0^2$, the change of linear refractive index for an isotropic film material is assumed to be [29,30]

$$\left(\frac{\partial n_0}{\partial\sigma}\right)_T = -\frac{1}{2}n_0^3\varphi \tag{8}$$

Consequently, a change in the linear refractive index due to film stress may affect the optical performance of an optical thin film, as shown in Eq. (8).

Fig. 9 shows the linear refractive indices and Young's moduli of Al_2O_3 films deposited at various pressures. The linear refractive index of Al_2O_3 film increased with Ar pressure. However, the stress of Al_2O_3 film decreased with

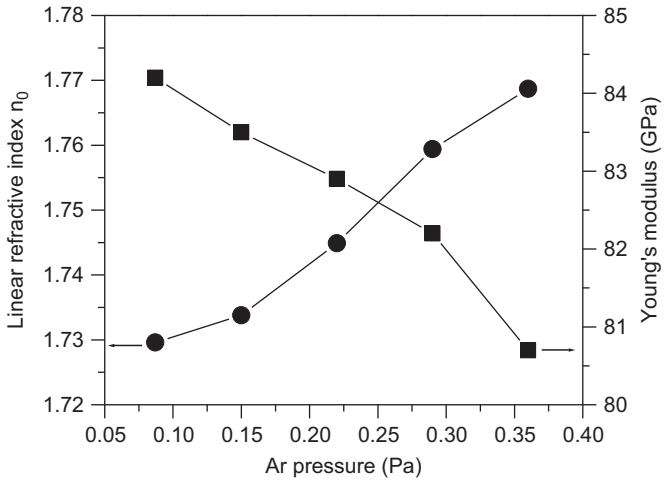

Fig. 9. The linear refractive indices and Young's moduli of Al_2O_3 films deposited at various pressures.

Ar pressure. The linear refractive index was found to correlate with the porosity [31,32]. It indicated that a dense Al_2O_3 film with a high linear refractive index and low stress could be obtained by increasing Ar pressure.

The value of $\Delta n/\Delta\sigma$ is reportedly similar to the stress-optical coefficient [33]. The stress-optical coefficient, $(\partial n_0/\partial\sigma)_T$, of the Al_2O_3 film was evaluated and was in the range of $-6.2\times10^{-12}\,Pa^{-1}$ to $-20.7\times10^{-12}\,Pa^{-1}$. Lower porosity corresponds to a lower stress-optical coefficient for the same material [32].

4. Conclusions

The fibered morphology and nanocrystallinity of Al_2O_3 film preferentially formed by decreasing Ar pressure. The hydrophilicity of Al_2O_3 film was enhanced by fibered morphology. The transmission in the VIS–NIR region of Al_2O_3 film increased with the decrease of Ar pressure. For the Al_2O_3 film deposited in a mixed Ar–O_2 atmosphere, the diffusion of oxygen into the grains could smooth the thin film and enhanced the transmission. The nonlinear refractive index of the Al_2O_3 film on the glass substrate was measured to be of the order of $10^{-8}\,cm^2\,W^{-1}$ and the change in the refractive index was of the order of 10^{-5}. The Al_2O_3 film exhibiting fibered morphology corresponded to higher optical energy gap and higher stress-optical coefficient.

Acknowledgements

The author would like to thank the National Science Council of the Republic of China, Taiwan, for financially supporting this research under Contract No. NSC-100–2221-E-260-014.

References

[1] S.M. Edlou, A. Smajkiewicz, G.A. Al-Jumaily, Optical properties and environmental stability of oxide coatings deposited by reactive sputtering, Applied Optics 32 (1993) 5601–5605.
[2] Y. Ao, Y. Yang, S. Yuan, H. Hu, H. Gu, G. Chen, Nanosized γ-Al_2O_3 protective film for fluorescent lamps, Ceramics International 33 (2007) 1547–1550.
[3] K. Koski, J. Hölsä, P. Juliet, Properties of aluminium oxide thin films deposited by reactive magnetron sputtering, Thin Solid Films 339 (1999) 240–248.
[4] F. Fietzke, K. Goedicke, W. Hempel, The deposition of hard crystalline Al_2O_3 layers by means of bipolar pulsed magnetron sputtering, Surface and Coatings Technology 86–87 (1996) 657–663.
[5] J. Wang, J. Binner, Y. Pang, B. Vaidhyanathan, Microwave-enhanced densification of sol–gel alumina films, Thin Solid Films 516 (2008) 5996–6001.
[6] A.K. Keshri, V. Singh, J. Huang, S. Seal, W. Choi, A. Agarwal, Intermediate temperature tribological behavior of carbon nanotube reinforced plasma sprayed aluminum oxide coating, Surface and Coatings Technology 204 (2010) 1847–1855.
[7] X. Duan, N.H. Tran, N.K. Roberts, R.N. Lamb, Single-source chemical vapor deposition of clean oriented Al_2O_3 thin films, Thin Solid Films 517 (2009) 5726–5730.
[8] M.M. Aslan, N.A. Webster, C.L. Byard, M.B. Pereira, C.M. Hayes, R.S. Wiederkehr, S.B. Mendes, Low-loss optical waveguides for the near ultra-violet and visible spectral regions with Al_2O_3 thin films from atomic layer deposition, Thin Solid Films 518 (2010) 4935–4940.
[9] N. Oka, R. Arisawa, A. Miyamura, Y. Sato, T. Yagi, N. Taketoshi, T. Baba, Y. Shigesato, Thermophysical properties of aluminum oxide and molybdenum layered films, Thin Solid Films 518 (2010) 3119–3121.
[10] M.J. Soileau, W.E. Williams, N. Mansour, E.W. Van Stryland, Laser-induced damage and the role of self-focusing, Optical Engineering 28 (1989) 1133–1144.
[11] E.W. Van Stryland, Y.Y. Wu, D.J. Hagan, M.J. Soileau, K. Mansour, Optical limiting with semiconductors, Journal of the Optical Society of America B 5 (1988) 1980–1988.
[12] M.J. Soileau, W.E. Williams, E.W. Van Stryland, Optical power limiter with picosecond response time, IEEE Journal of Quantum Electronics QE-19 (1983) 731–735.
[13] K. Mansour, M.J. Soileau, E.W. Van Stryland, Nonlinear optical properties of carbon-black suspensions (ink), Journal of the Optical Society of America B 3 (1992) 1100–1109.
[14] S.V. Prasad, S.D. Walck, J.S. Zabinski, Microstructural evolution in lubricious ZnO films grown by pulsed laser deposition, Thin Solid Films 360 (2000) 107–117.
[15] G. Knuyt, C. Quaeyhaegens, J. D'Haen, L.M. Stals, A quantitative model for the evolution from random orientation to a unique texture in PVD thin film growth, Thin Solid Films 258 (1995) 159–169.
[16] G. Knuyt, C. Quaeyhaegens, J. D'Haen, L.M. Stals, A model for thin film texture evolution driven by surface energy effects, Physica Status Solidi B 195 (1996) 179–193.
[17] P.B. Barna, M. Adamik, Fundamental structure forming phenomena of polycrystalline films and the structure zone models, Thin Solid Films 317 (1998) 27–33.
[18] D. Wang, U. Geyer, S. Schneider, G.V. Minnigerode, Grain sizes of Ni films measured by STM and X-ray methods, Thin Solid Films 292 (1997) 184–188.
[19] M. Ohring, The Materials Science of Thin Films, Academic Press, San Diego, CA, 1991, p. 111.
[20] S.S. Lin, J.L. Huang, Microstructure and optical properties of AlOx thin films grown on ZnO-deposited glass, Journal of Materials Research 18 (2003) 1943–1949.
[21] A.S. Guzenda, M.G. Lipman, H. Szymanowski, J. Kowalski, P. Wojciechowski, T. Halamus, A. Tracz, Characterization of thin TiO_2 films prepared by plasma enhanced chemical vapour deposition for optical and photocatalytic applications, Thin Solid Films 517 (2009) 5409–5414.
[22] I. Bernagozzi, S. Torrengo, L. Minati, M. Ferrari, A. Chiappini, C. Armellini, L. Toniutti, L. Lunelli, G. Speranza, Synthesis and characterization of PMMA-based superhydrophobic surfaces, Colloid and Polymer Science 290 (2012) 315–322.
[23] M. Ohring, The Materials Science of Thin Films, Academic Press, San Diego, CA, 1991, p. 509.
[24] N. Serpone, D. Lawless, R. Khairutdinov, Subnanosecond relaxation dynamics in TiO_2 colloidal sols (particle sizes Rp=1.0–13.4 nm). Relevance to heterogeneous photocatalysis, Journal of Physical Chemistry 99 (1995) 16655–16661.
[25] D.D. Claudio, A.R. Phani, S. Santucci, Enhanced optical properties of sol–gel derived TiO_2 films using microwave irradiation, Optical Materials 30 (2007) 279–284.
[26] B.E. Sernelius, K.F. Berggren, Z.C. Jin, I. Hamberg, C.G. Granqvist, Band-gap tailoring of ZnO by means of heavy Al doping, Physical Review B 37 (1988) 10244–10248.
[27] E. Mollwo, in: R.G. Breckenridge, B.R. Russell, E.E. Hahn (Eds.), Proc. Photoconductivity Conf., Wiley, New York, 1954, p. 509.
[28] M. Bender, W. Seelig, C. Daube, H. Frankenberger, B. Ocker, J. Stollenwerk, Dependence of oxygen flow on optical and electrical properties of DC-magnetron sputtered ITO films, Thin Solid Films 326 (1998) 72–77.
[29] J.F. Nye, Physical Properties of Crystals: Their Representation by Tensors and Matrices, Oxford Science, New York, 1992.

[30] W. Lukosz, P. Pliska, Determination of thickness, refractive indices, optical anisotropy of, and stresses in SiO_2 films on silicon wafers, Optics Communications 117 (1995) 1–7.
[31] G.S. Vicente, A. Morales, M.T. Gutierrez, Preparation and characterization of sol–gel TiO_2 antireflective coatings for silicon, Thin Solid Films 391 (2001) 133–137.
[32] S.S Lin, D.K. Wu, Enhanced optical properties of TiO_2 nanoceramic films by oxygen atmosphere, Journal of Nanoscience and Nanotechnology 10 (2010) 1099–1104.
[33] B. Hunsche, M. Vergöhl, H. Neuhäuser, F. Klose, B. Szyszka, T. Matthée, Effect of deposition parameters on optical and mechanical properties of MF- and DC-sputtered Nb_2O_5 films, Thin Solid Films 392 (2001) 184–190.